Physica E 120 (2020) 114052

Contents lists available at ScienceDirect

Physica E: Low-dimensional Systems and Nanostructures

journal homepage: http://www.elsevier.com/locate/physe

Nonequilibrium magnetic properties of the mixed spin (1/2, 1) Ising nanowire with core-shell structure

Bayram Deviren

Department of Physics, Nevsehir Hacı Bektaş Veli University, 50300, Nevsehir, Turkey

ARTICLE INFO

Keywords:
nanowire
Nonequilibrium phase transitions
Nonequilibrium magnetic properties
Glauber-type stochastic dynamics

ABSTRACT

The nonequilibrium magnetic properties (phase transition temperatures, phase diagrams, hysteresis loop areas and correlations) are investigated in the kinetic mixed spin (1/2, 1) Ising nanowire system under the time varying magnetic field. The Glauber-type stochastic dynamics are employed to construct the set of mean field dynamic equations. The time variation of the core/shell magnetizations and the thermal behavior of the dynamic core/shell magnetizations are examined, extensively. The dynamic core/shell magnetizations, hysteresis loop areas and correlations are studied as a function of temperature in order to characterize the nature (continuous or discontinuous) of the phase transitions as well as to find the dynamic phase transition temperatures. The dynamic phase diagrams are presented in the magnetic field amplitude and temperature plane. The dynamic phase diagrams exhibit paramagnetic (p), ferrimagnetic (i), nonmagnetic (nm) phases, three mixed regions, (i + nm), (i + p) and (nm + p). The dynamic phase diagrams contain a dynamic tricritical point and reentrant phenomena, which strongly depend on interaction parameters.

1. Introduction

With the development of new nanotechnologies, magnetic nanostructured materials, such as nanowires [1], nanotubes [2], nanofilms [3], nanorods [4], and nanoparticles [5] have attracted growing interest for both experimental and theoretical researchers over the last decades because of their fascinating mechanical, electrochemical, optical, piezoelectrical properties [6–8] and technological applications from a wide range of disciplines, including biomedical applications, nonlinear optics, magnetic recording media, environmental remediation, information data storage, sensors, bio-separation, catalysis, magnetic particle imaging, biotechnology, nanofluids and propagation losses [9–13]. In particular, magnetic nanowires exhibit diversified amount of different magnetic properties such as extra single ion anisotropy contributions, superparamagnetism, high saturation field, high field irreversibility as compared with those in respective bulk materials and greatly affected by the particle size [14]. These phenomena originate from the surface effects and finite size that influence the magnetic behavior of individual nanowires [15].

Much effort has been dedicated to provide a better understanding of the magnetic behavior of nanowires analytically [16], experimentally [17], and in computer simulations [18]. Magnetic nanowires have also fabricated by using a diverse range of fabrication techniques, such as ultrashort laser ablation [19], trioctylamine solution method [20], electrodeposition using anodized aluminum oxide templates [21] and direct-current electrodeposition [22]. Theoretically, the Ising model with core/shell structure has been accepted and applied successfully to explain many characteristic phenomena in magnetic nanomaterials such as magnetic nanoparticles, nanotubes and nanowires [23–30]. Moreover, the equilibrium thermal and magnetic behavior of various types of magnetic nanowires have been studied by use of the several statistical physics methods, including mean-field approximation (MFA) [31], effective field theory (EFT) with correlations [32], Green function formalism [33], Bethe Peierls approximation [34], Monte Carlo simulation (MCS) [35], and Bethe lattice approximation [36]. More recently, Boughrara et al. [37] have investigated the phase diagrams and magnetic behaviors of the mixed spin (1/2, 1) Ising nanowire and they have obtained the phase diagrams of the system which include very rich critical behaviors, i.e., the first-, second-order phase transitions and a compensation point depending on the values of interaction parameters. Boughrara et al. [38] have also applied MCS to examine the phase diagrams (critical and compensation temperatures) of a mixed spin (1/2, 1) Ising nanowire with a negative core–shell interaction and a surface dilution. The phase diagrams of this system exhibit the first-, second-order phase transitions, tricritical point and critical end point. Albayrak [39] has studied the core–shell structured square mixed spin

E-mail address: bayram.deviren@nevsehir.edu.tr.

https://doi.org/10.1016/j.physe.2020.114052
Received 20 September 2019; Received in revised form 16 January 2020; Accepted 25 February 2020
Available online 2 March 2020

(1/2, 1) Ising nanowire on the Bethe lattice by using the exact recursion relations. The obtained phase diagrams show both the first-, second-order phase transitions and tricritical points for the appropriate values of interaction parameters.

Although the equilibrium behavior of nano-structure systems has been extensively investigated and is well understood, the mechanism behind the statistical properties of non-equilibrium systems has not yet been explored and is less developed intensively. The reason of this is that the magnetically interacting systems under the influence of sinusoidally time dependent oscillating magnetic field display some significant behaviors: dynamic phase transitions, dynamic phase diagrams, dynamic hysteresis loop areas and correlations. In particular, the kinetic Ising model was proposed as a simplified model for the analysis of a great variety of interacting systems such as chemical reactions, domain growth, contact process, catalysis and transport phenomena. The dynamic phase transition was first introduced in the kinetic spin-1/2 Ising model in the presence of a time-dependent oscillating field by using the MFT based on Glauber dynamics [41]. Then a great deal of studies concerning the dynamic phase transitions of various types of magnetic systems have been studied by a different of techniques such as MFT [42–45], MCS [46,47], EFT [48,49], real space renormalization group technique [50] and using recursion relations on the Bethe lattice [51]. Not only is it an exciting system from a merely theoretical point of view, but also the kinetic Ising model can be carried out to describe experimental evidence in highly anisotropic (Ising-like) and ultra thin Co/Cu (001) ferromagnetic films [52], a $[Co/Pt]_3$ magnetic multilayer system with strong perpendicular anisotropy [53], amorphous YBaCuO films [54], nanocomposites [55]. We should also mentioning that the dynamic behaviors of the single spin Ising nanostructured system have investigated by using the various methods [56,57]. We should also mention that various type of cylindrical Ising nanowire systems in an oscillating magnetic field have been investigated by using the MFT based on Glauber type stochastic dynamics [58–61]. Therefore, the method used in this study is a reliable and feasible to understand the nonequilibrium magnetic behavior of different magnetic systems.

As far as we know, the non-equilibrium magnetic behaviors of the mixed spin (1/2, 1) Ising nanowire have not yet been investigated. The dynamic investigations on the magnetic nanosystem constitute an important role in the real magnetic material science, since the surface effects, crystal field and sinusoidally oscillating magnetic field may induce some important microscopic influences on the material. Therefore, we believe that the investigation of the effects of crystal field, exchange interactions and magnetic field on the nonequilibrium magnetic behavior of the Ising nanostructured system and its derivations still need particular attention. Hence, in this work based on MFA with the Glauber dynamics, we intend to investigate the nonequilibrium properties of a mixed spin (1/2, 1) Ising nanowire with core-shell structure in the presence of a time-dependent magnetic field. In this way, the dynamic core/shell magnetizations, hysteresis loop areas and correlations are studied as a function of temperature in order to characterize the nature (continuous or discontinuous) of the phase transitions as well as to find the dynamic phase transition temperatures. As a result, the dynamic phase diagrams of the system are presented in the magnetic field amplitude and temperature plane.

The outline of the remaining part of this paper is as follows. In Section 2, the model is briefly described and formulation is given. Section 3 is devoted to the numerical results and discussions. Finally, the paper ends with summary and conclusions in Section 4.

2. Model and formulations

The MFA method with the Glauber type stochastic dynamics is applied to investigate the nonequilibrium magnetic behavior of the complex spin systems, such as the ferrimagnetic mixed spin (1/2, 1) Ising nanowire. The model of our interest consists of four sublattices A, B, C and D, which arranged alternatively. The first two sublattices A and B are occupied by spins σ assumed to take the values ± 1/2, while the last two sublattices C and D are occupied by the spins *S* which takes the values ± 1, 0. The schematic representation of our model with core-shell structure is depicted in Fig. 1. The sites of the core are occupied by σ spins, while those of shell are occupied by *S* spins. Each spin is connected to the nearest-neighbor spins with the exchange interaction parameters.

The Hamiltonian of the mixed spin (1/2, 1) Ising nanowire with a crystal-field interaction (D) in the presence of a time dependent oscillating external magnetic field is given by

$$H = -J_C\sum_{\langle ij\rangle}\sigma_i\sigma_j - J_S\sum_{\langle mn\rangle}S_mS_n - J_{Int}\sum_{\langle kl\rangle}\sigma_kS_l - D\sum_{\langle m\rangle}S_m^2 + h(t)\left(\sum_i\sigma_i + \sum_m S_m\right), \quad (1)$$

where J_C and J_S are the exchange interaction parameters between the two nearest-neighbor magnetic particles at the core and shell, respectively, and J_{Int} is the interaction parameters between the two nearest-neighbor magnetic particles at the shell and core. The summations over all pairs of neighboring spins at the core, shell and between core and shell are denoted by the indexes <ij>, <mn> and <kl>, respectively. The surface exchange interaction is often defined as $J_S = J_C(1 + \Delta_S)$. Δ_S is used to clarify the effects of surface and core interactions on the physical properties in the system. We also define a coupling parameter r as $r = \frac{J_{int}}{J_c}$ $h(t)$ is an oscillating magnetic field and is given by

$$h(t) = h_0\sin(wt), \quad (2)$$

where h_0 and $w = 2\pi\nu$ are the amplitude and the angular frequency of the oscillating field, respectively. The system is in contact with an isothermal heat bath at absolute temperature T_A.

The Glauber-type stochastic dynamics is applied to achieve the set of the mean-field dynamic equations. Thus, the system evolves at a rate of $1/\tau$ transitions per unit time according to a Glauber-type stochastic process. The MFA with Glauber-type stochastic dynamics are known to be effective in many physical relevant situations as mentioned in the introduction. The mathematical justifications of such approximations rely generally on specific considerations which depend too much on the model and on the initial states of the system which are required to be well-prepared. This kind of mean-field dynamic study, in spite of its simplicity and limitations such as the correlations of spin fluctuations have not been considered, is an adequate starting point from which easy to determine the complete dynamic phase diagrams. Since the derivation of the dynamic MF equations was explained exhaustively for spin-1/2 system [40] and different spin systems [42–45], in here, we shall only give a brief summary. The spins are assumed to interact not only with the neighbors and oscillating external magnetic field but also with heat bath, based on the Glauber-type stochastic dynamics. Let us define the $P_{c1}(\sigma_1, \sigma_2, ..., \sigma_N; t)$, $P_{c2}(\sigma_1, \sigma_2, ..., \sigma_N; t)$, $P_{s1}(S_1, S_2, ..., S_N; t)$ and $P_{s2}(S_1, S_2, ..., S_N; t)$ as the probabilities per unit time that the center core *c1*, the core *c2*, and the shells *s1*, *s2*, respectively. Then the master equation for the first σ-spins, which located at the center of the nanowire, can be written as

$$\frac{d}{dt}P_{c1}(\sigma_1, \sigma_2, ..., \sigma_N; t) = -\sum_i W_i(-\sigma_i)\ P_{c1}(\sigma_1, \sigma_2, ..., \sigma_i, ...\sigma_N; t) + \sum_i W_i(\sigma_i)\ P_{c1}(\sigma_1, \sigma_2, ..., -\sigma_i, ...\sigma_N; t). \quad (3)$$

where $W_i(\sigma_i)$ is the probability per unit time that the *i*th σ spin changes from σ_i to $-\sigma_i$ (while the spins on other sublattice momentarily fixed). Each spin σ can flip with the probability per unit time given by the Boltzman factor; moreover, it is easy to prove that the averages satisfy the equations:

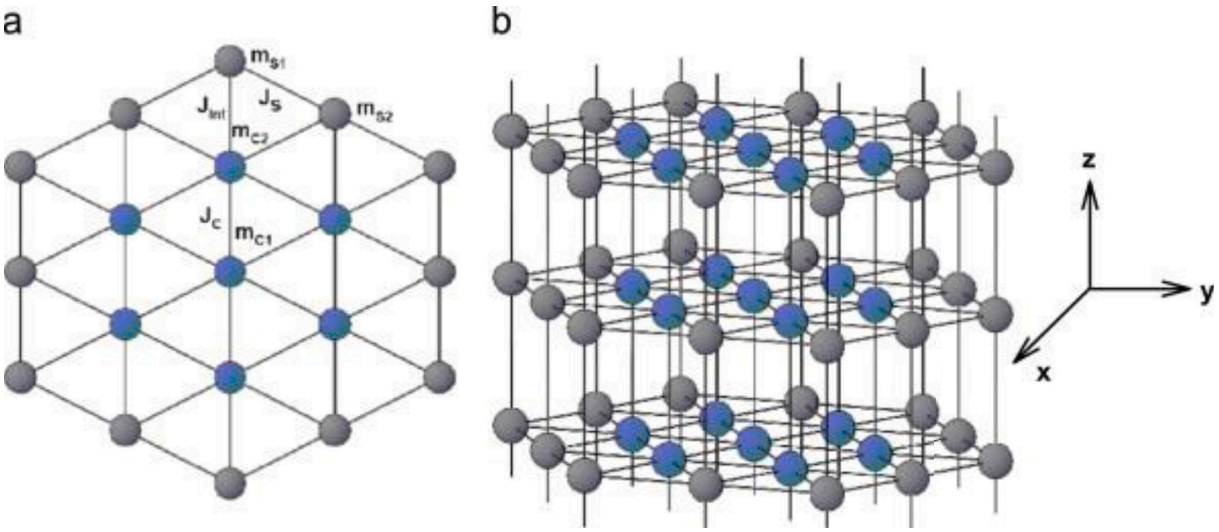

Fig. 1. Schematic representation of a nano-hegzagonal structure. The grey and blue circles indicate magnetic atoms at the surface shell and core, respectively. (a) cross-section, (b) three-dimensional. (For interpretation of the references to colour in this figure legend, the reader is referred to the Web version of this article.)

$$\Omega \frac{d}{d\xi} m_{c1} = -m_{c1} + \frac{1}{2}\tanh\left[\frac{\beta}{2}\left(2\ J_C\ m_{C1} + 6\ J_C\ m_{C2} + h_0 \sin(\xi)\right)\right] \tag{4}$$

We can also obtain the other mean-field dynamical equations for the other spins on the mixed spin Ising nanowire system by using the similar calculations as follows;

$$\Omega \frac{d}{d\xi} m_{c2} = -m_{c2} + \frac{1}{2}\tanh\left[\frac{\beta}{2}\left(J_C\ m_{c1} + 4\ J_C\ m_{c2} + J_{Int}\ m_{s1} + 2\ J_{Int}\ m_{s2} + h_0 \sin(\xi)\right)\right] \tag{5}$$

$$\Omega \frac{d}{d\xi} m_{s1} = -m_{s1} + \frac{2\sinh[\beta(J_{Int}\ m_{c2} + 2\ J_S\ m_{s1} + 2\ J_S\ m_{s2} + h_0 \sin(\xi))]}{2\cosh[\beta(J_{Int}\ m_{c2} + 2\ J_S\ m_{s1} + 2\ J_S\ m_{s2} + h_0 \sin(\xi))] + \exp(-\beta D)}, \tag{6}$$

$$\Omega \frac{d}{d\xi} m_{s2} = -m_{s2} + \frac{2\sinh[\beta(2\ J_{Int}\ m_{c2} + 2\ J_S\ m_{s1} + 2\ J_S\ m_{s2} + h_0 \sin(\xi))]}{2\cosh[\beta(2\ J_{Int}\ m_{c2} + 2\ J_S\ m_{s1} + 2\ J_S\ m_{s2} + h_0 \sin(\xi))] + \exp(-\beta D)}, \tag{7}$$

where $m_{c1} = \langle\sigma_i\rangle$, $m_{c2} = \langle\sigma_j\rangle m_{s1} = \langle S_m\rangle$, $m_{s2} = \langle S_n\rangle$, $\xi = \mathrm{w}\,t$, and $\Omega = \tau\,\mathrm{w} = 2\pi$. Thus, the set of the mean-field dynamical equations for the average magnetizations are obtained, namely Eqs. (4)–(7). These equations are solved numerically by using the Adams Moulten predicter corrector method with Simpson integration. In the general case, the solutions of the equations depend on the initial conditions of the core and shell magnetizations.

The dynamic order parameters or dynamic magnetizations as the time-averaged magnetization over a period of the oscillating magnetic field are given as

$$M_\alpha = \frac{\mathrm{w}}{2\pi}\oint m_\alpha(t)\ dt\ , \tag{8}$$

where $\alpha = c1, c2, s1, s2$ which correspond to the dynamic magnetizations on the system. On the other hand, the hysteresis loop areas are defined by Acharyya [62] as

$$A_\alpha = -\oint m_\alpha(t)\ dh = -h_0 \mathrm{w}\oint m_\alpha(t)\cos(\mathrm{w}t)dt, \tag{9}$$

which correspond to the energy loss due to the hysteresis. The dynamic correlations are calculated as

$$C_\alpha = \frac{\mathrm{w}}{2\pi}\oint m_\alpha(t)\ h(t)dt = \frac{\mathrm{w}h_0}{2\pi}\oint m_\alpha(t)\sin(\mathrm{w}t)dt. \tag{10}$$

We should also mention that in the numerical calculations, the hysteresis loop areas A_α and the dynamic correlations C_α are also measure in units J_C. In the next section, we will give the numerical results of these equations.

3. Numerical results and discussions

3.1. Time variations of the average order parameters

In this section, first we study the time variations of the average magnetizations to find the phases in the system. In order to investigate the behaviors of time variations of the average magnetizations, we have to study the stationary solutions of the set of coupled dynamical mean-field equations, given in Eqs. (4)–(7), when the parameters J_C, J_S, J_{Int}, T and h are varied. The stationary solutions of these equations will be a periodic function of ξ with period 2π; that is, $m_{c1}(\xi + 2\pi) = m_{c1}(\xi)$, $m_{c2}(\xi + 2\pi) = m_{c2}(\xi)$, $m_{s1}(\xi + 2\pi) = m_{s1}(\xi)$ and $m_{s2}(\xi + 2\pi) = m_{s2}(\xi)$. Moreover, they can be one of three types according to whether they have or do not have the properties

$$m_{c1}(\xi + \pi) = -\ m_{c1}(\xi), \tag{11a}$$

$$m_{c2}(\xi + \pi) = -\ m_{c2}(\xi), \tag{11b}$$

$$m_{s1}(\xi + \pi) = -\ m_{s1}(\xi), \tag{11c}$$

$$m_{s2}(\xi + \pi) = -\ m_{s2}(\xi), \tag{11d}$$

The first type of solution satisfies Eq. (11) is called a symmetric solution which corresponds to a paramagnetic (p) solution. In this solution, the magnetizations are equal to each other ($m_{c1}(\xi) = m_{c2}(\xi) = m_{s1}(\xi) = m_{s2}(\xi)$) and they oscillate around zero and are delayed with respect to the external magnetic field. The second type of solution, which does not satisfy Eq. (11), is called a nonsymmetric solution that corresponds to a ferrimagnetic (i) solution. In this solution, the $m_{c1}(\xi)$ and $m_{c2}(\xi)$ are equal to each other ($m_{c1}(\xi) = m_{c2}(\xi) = \pm 0.5$), and they do not follow the external magnetic field any more, and instead of oscillating around zero, they oscillate around nonzero values, namely ± 0.5; but the $m_{s1}(\xi)$ and $m_{s2}(\xi)$ are equal to each other and oscillate

around ± 1.0 ($m_{s1}(\xi) = m_{s2}(\xi) = \pm 1.0$); hence, the system has the ferrimagnetic (i) phase. The third type of solution, which does not satisfy Eq. (11a) and Eq. (11a), and satisfy Eq. (11c) and Eq. (11d); this solution corresponds to a nonmagnetic (nm) solution; because the ($m_{c1}(\xi) = m_{c2}(\xi) = \pm 0.5$) and ($m_{s1}(\xi) = m_{s2}(\xi) = 0.0$). These facts are seen explicitly by solving Eqs. (4)–(7) using the Adams-Moulton predictor-corrector method for a given set of parameters and initial values, and obtained results are presented in Fig. 2. From Fig. 2, one can see following six different solutions or phases, namely the p, i and nm fundamental solutions, and three coexistence state or solutions, namely the i + nm in which i and nm solutions coexist; the i + p in which i and p solutions coexist; the nm + p in which nm and p solutions coexist, have been found. In Fig. 2(a) only the symmetric solution is always obtained, in this case ($m_{c1}(\xi) = m_{c2}(\xi) = m_{s1}(\xi) = m_{s2}(\xi)$) oscillate around zero value ($m_{c1}(\xi) = m_{c2}(\xi) = m_{s1}(\xi) = m_{s2}(\xi) = 0.0$). Hence, we have paramagnetic (p) solution. On the other hand, in Fig. 2 (b) only the

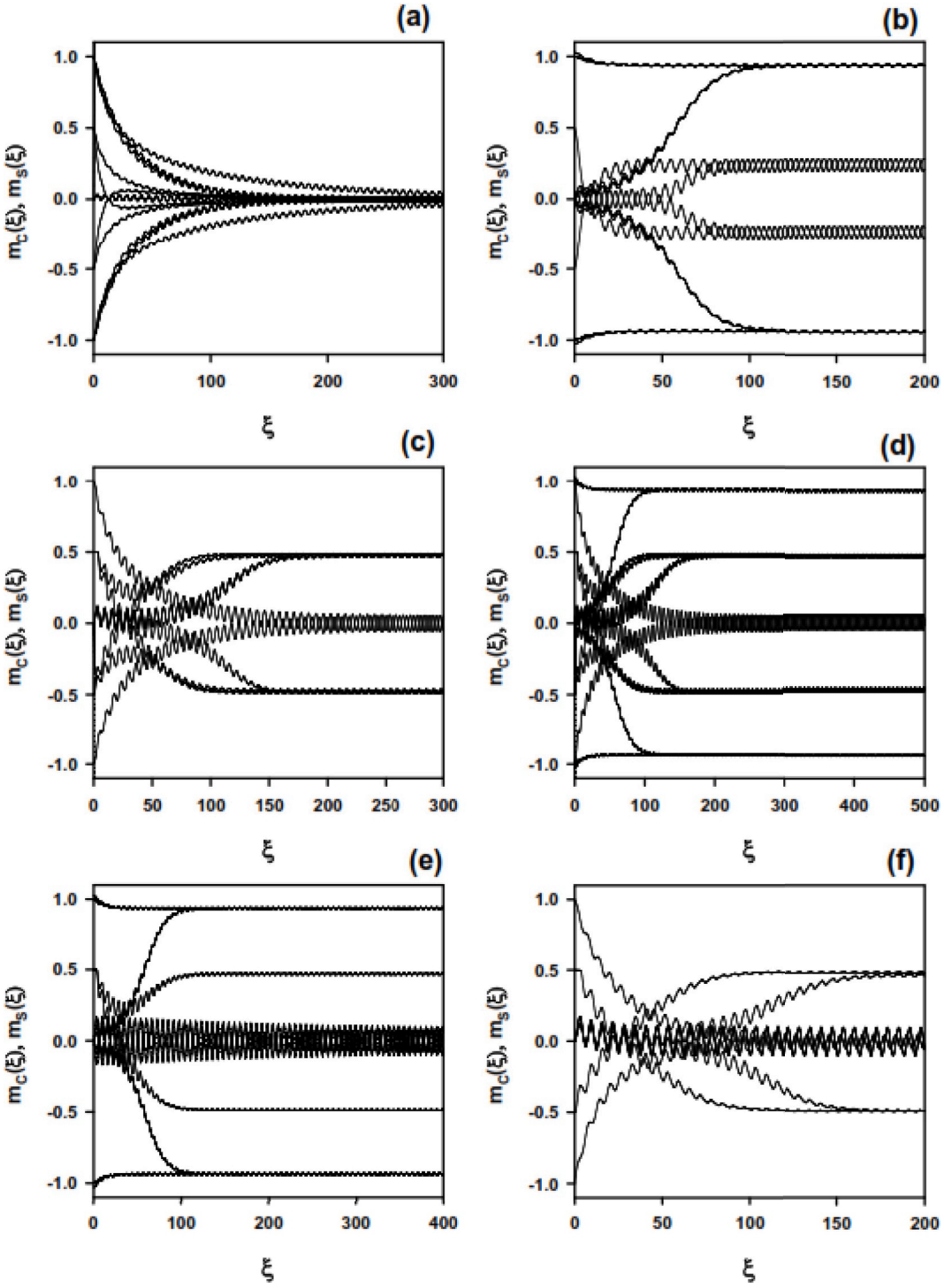

Fig. 2. Time variations of the average magnetizations for the mixed spin (1/2, 1) Ising nanowire system at $\Delta_S = 0.0$, $r = 1.0$. **a)** Exhibiting a paramagnetic (p) phase: $D = -4.0$, $h = 3.0$ and $T = 1.5$. **b)** Exhibiting a ferrimagnetic (i) phase: $D = 1.0$, $h = 2.0$ and $T = 2.25$. **c)** Exhibiting a nonmagnetic (nm) phase: $D = -3.3$, $h = 1.0$ and $T = 1.25$. **d)** Exhibiting a coexistence region (i + nm): $D = -3.2$, $h = 0.5$ and $T = 0.30$. **e)** Exhibiting a coexistence region (i + p): $D = -2.5$, $h = 2.0$ and $T = 0.10$. **f)** Exhibiting a coexistence region (nm + p): $D = -5.0$, $h = 2.0$ and $T = 0.15$.

nonsymmetric solution is found; therefore, we have the i solution. In Fig. 2(b), $m_{c1}(\xi)$ and $m_{c2}(\xi)$ oscillate around ± 0.5 and $m_{s1}(\xi)$ and $m_{s2}(\xi)$ oscillate around ± 1; hence we have the ferrimagnetic (i) phase ($m_{c1}(\xi) = m_{c2}(\xi) = \pm 0.5,\ m_{s1}(\xi) = m_{s2}(\xi) = \pm 1.0$). In Fig. 2(c), the system represents both the symmetric and nonsymmetric solutions; hence we have the nm phase. In Fig. 2(c), $m_{c1}(\xi)$ and $m_{c2}(\xi)$ oscillate around ± 0.5, and $m_{s1}(\xi)$ and $m_{s2}(\xi)$ oscillate around zero, this solution corresponds to the nonmagnetic (nm) phase ($m_{c1}(\xi) = m_{c2}(\xi) = \pm 0.5,\ m_{s1}(\xi) = m_{s2}(\xi) = 0.0$). In Fig. 2(d), $m_{c1}(\xi)$ and $m_{c2}(\xi)$ oscillate around either ± 0.5 and $m_{s1}(\xi)$ and $m_{s2}(\xi)$ oscillate around either ± 1, that corresponds to the i phase; or $m_{c1}(\xi)$ and $m_{c2}(\xi)$ oscillate around either ± 0.5 and $m_{s1}(\xi)$ and $m_{s2}(\xi)$ oscillate around zero, that corresponds to the nm phase; depend on the initial values of the system parameters; hence we have the coexistence solution (i + nm), as explained above. In Fig. 2(e), $m_{c1}(\xi)$ and $m_{c2}(\xi)$ oscillate around either ± 0.5 and $m_{s1}(\xi)$ and $m_{s2}(\xi)$ oscillate around either ± 1, that corresponds to the i phase, or they oscillate around zero which corresponds to the p phase depend on the initial values of the system parameters; hence we have the coexistence solution (i + p), as explained above. In Fig. 2(f), $m_{c1}(\xi)$ and $m_{c2}(\xi)$ oscillate around either ± 0.5; $m_{s1}(\xi)$ and $m_{s2}(\xi)$ oscillate around zero, that corresponds to the nm phase, or oscillate around zero value which corresponds to the p phase which also depend on the initial values of the system parameters; hence we have the coexistence solution (nm + p). Fig. 2(a–c) does not depend on the initial values, but the other solutions depend on the initial values.

3.2. *Thermal behavior of the dynamic magnetizations, hysteresis loop areas and correlations*

In this section, we investigate the behavior of the dynamic magnetizations (M_α), hysteresis loop areas (A_α) and correlations (C_α) as a function of the temperature on the mixed spin (1/2, 1) Ising nanowire system for several values of interaction parameters and crystal field interaction in the presence of the external magnetic field. In order to investigate the thermal behavior of the M_α, A_α and C_α, we solve Eqs. (8)-(10) by combining the numerical methods of Adams-Moulton predictor

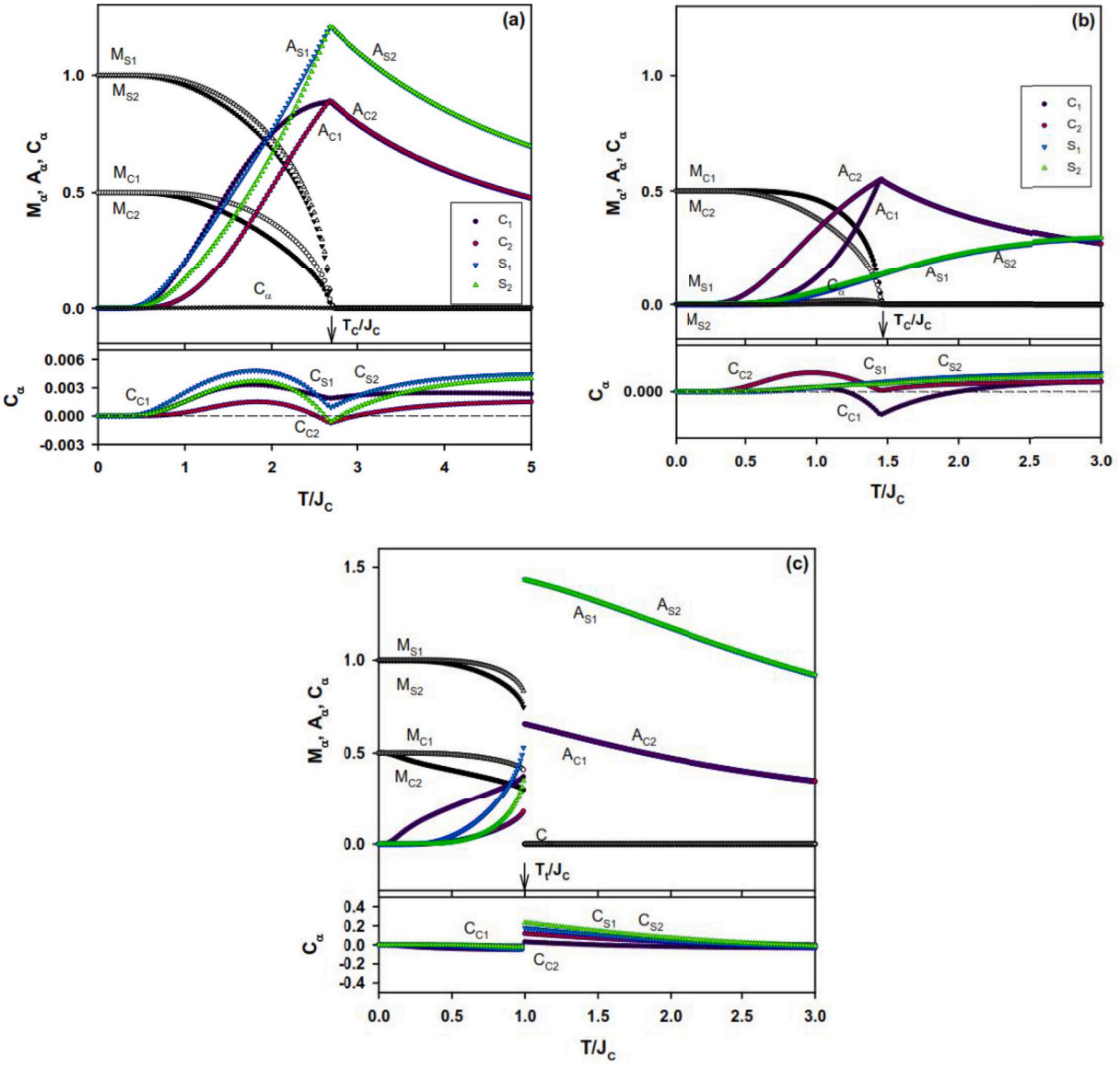

Fig. 3. (Colour Online) Thermal variations of the dynamic magnetizations for the various values of D and h. T_C/J_C and T_t/J_C are the second- and first-order phase transition temperatures, respectively. **a)** Exhibiting a second-order phase transition from the ferrimagnetic (i) phase to the paramagnetic (p) phase for $D = -2.5$ and $h = 0.5$; $T_C/J_C = 2.685$ is found. **b)** Exhibiting a second-order phase transition from the nonmagnetic (nm) phase to the paramagnetic (p) phase for $D = -3.3$ and $h = 1.6$; $T_C/J_C = 1.455$ is found. **c)** Exhibiting a second-order phase transition from the nonmagnetic (nm) phase to the paramagnetic (p) phase for $D = -3.3$ and $h = 1.6$; $T_C/J_C = 1.455$ is found. (For interpretation of the references to colour in this figure legend, the reader is referred to the Web version of this article.)

corrector method with the Romberg integration. This study leads us to characterize the nature (continuous or discontinuous) of DPTs, to check the stability of each dynamical phase, as well as to obtain the DPT points. A few explanatory and interesting results are plotted in Figs. 3 and 4 to illustrate the calculation of the DPT points. Fig. 3(a) illustrates the thermal variation of the M_α, A_α and C_α for $\Delta_S = 0.0$, $r = 1.0$, $D = 1.0$ and $h = 2.75$. In this figure, the dynamic magnetizations are $M_{c1} = M_{c2} = 0.5$ and $M_{s1} = M_{s2} = 1.0$ at zero temperature, and they go to zero continuously as the temperature increases; therefore, a second-order phase transition occurs at $T_C/J_C = 2.685$ and the DPT is from the ferrimagnetic (i) phase to the paramagnetic (p) phase. We have checked the stability of DPT points between the phases of the system by investigating the A_α and C_α. The A_α and C_α become a maximum and a minimum (negative) at the second-order phase transition temperature T_C/J_C, respectively. This has also been tested by our calculations, because we have found exactly the same critical temperature (T_C/J_C) for these calculations. Fig. 3(b) is plotted for $\Delta_S = 0.0$, $r = 1.0$, $D = -3.3$ and $h = 1.6$. In Fig. 3(b), $M_{c1} = M_{c1} = 0.5$ and $M_{s1} = M_{s2} = 0.0$ at the zero temperature and the core magnetizations go to zero continuously as the temperature increases; therefore, a second-order phase transition occurs at $T_C/J_C = 1.455$ and the DPT is from the nonmagnetic (nm) phase to the paramagnetic (p) phase. While the A_{c1}, A_{c2} and C_{c1}, C_{c2} for the core represent the similar behavior to the one seen in Fig. 3(a), the A_{s1}, A_{s2} and C_{s1}, C_{s2} for the shell show an increasing behavior from zero to positive values. Fig. 3(c) is represented for $\Delta_S = 0.0$, $r = 1.0$, $D = 1.0$ and $h = 3.75$. In Fig. 3(c), $M_{c1} = M_{c1} = 0.5$ and $M_{s1} = M_{s2} = 1.0$ at the zero temperature and the magnetizations go to zero discontinuously as the temperature increases; hence, the system undergoes a first-order phase transition from the i phase to the p phase at $T_t/J_C = 1.025$. Therefore, T_t/J_C is the first-order phase transition temperature where the discontinuity or jump occurs. We also checked this dynamic discontinuous transition by investigating the thermal behavior of the dynamic hysteresis loop areas A_α and dynamic correlations C_α. From the figure, one can see that if the temperature increases from zero, the A_α and C_α increase and decrease from zero to a certain positive non zero values, and A_α and C_α suddenly jump to the higher positive and lower negative values, respectively; hence, the first order phase transition occur at $T_t/J_C = 1.025$, which is exactly the first-order phase transition that is found by investigation of the thermal behavior of the M_α, A_α and C_α.

The temperature dependence of M_α, A_α and C_α are plotted in order to see the phase transition from the mixed i + p phase to the i phase and then the p phase for $\Delta_S = 0.0$, $r = 1.0$, $D = -2.5$ and $h = 0.5$ and various initial values, seen in Fig. 4. The behavior of Fig. 4(a) is similar to Fig. 3 (a); hence the system undergoes a second-order phase transition from the i phase to the p phase at $T_C/J_C = 2.025$. In Fig. 4(b), the system undergoes two successive phae transitions. The first one is a first-order, because the discontinuous occurs for M_α, A_α and C_α at $T_t/J_C = 0.65$. Transition is from the nm phase to the i phase. The second one is a second-order from the i phase to the p phase at $T_C/J_C = 2.025$. Therefore, the coexistence region i.e., the mixed phase exists in the system. If one compares Fig. 4(a) and (b) with Fig. 5(c), the system exhibits the mixed i + nm phase until $T_t/J_C = 0.65$, the i phase between at $T_t/J_C = 0.65$ and at $T_C/J_C = 2.025$, the p phase after $T_C/J_C = 2.025$. By investigating the A_α and C_α, the stability of DPT between the phases in the system have been checked; because the same critical temperature for these calculations have exactly been found. Two successive phase transitions were also experimentally observed in $DyVO_4$ [63,64] and in TbB_4 at $T_{N1} = 24$ K and $T_{N2} = 44$ K in the magnetic susceptibility measurements [65]. Moreover, two successive transitions have also been theoretically found on the magnetic properties of the various Ising systems, using the different method [42–45,49,66].

3.3. The dynamic phase diagrams

We can now present the dynamic phase diagrams of the system, since we have characterized the nature of DPTs and obtained the DPT points in subsection 3.2. The calculated phase diagrams in the (T/J_C, h/J_C) plane are presented in Fig. 5 for $\Delta_S = 0.0$, $r = 1.0$ and various values of crystal field (D). In these phase diagrams the solid and dashed lines represent the dynamic second- and first-order phase transition lines, respectively, and the dynamic tricritical point is denoted by a filled circle. As seen in Fig. 5, seven different types of phase diagram topologies have been observed.

(i) Fig. 5(a) is performed for $D = 1.0$, and in the phase diagram, at high temperature (T) and high external magnetic field (h), the

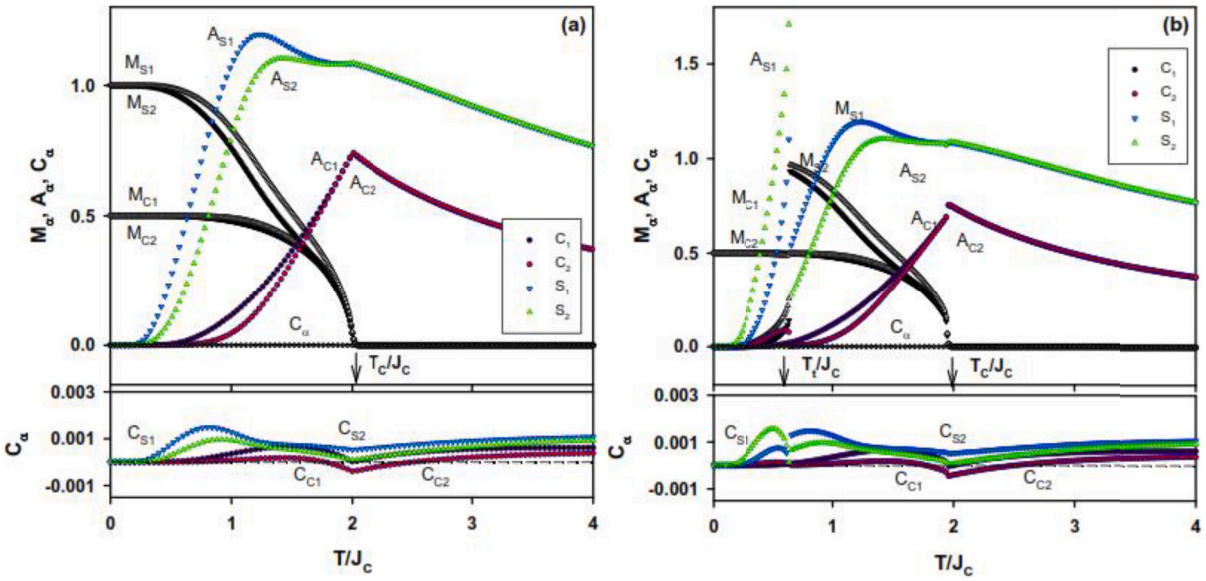

Fig. 4. (Colour Online) Thermal variations of the dynamic magnetizations for the various values of D = −2.5 and $h = 0.5$. T_C/J_C and T_t/J_C are the second- and first-order phase transition temperatures, respectively. **a)** Exhibiting a dynamic second-order phase transition from the i phase to the p phase for $D = -2.5$ and $h = 0.5$ and the initial values of $M_{c1} = M_{c2} = 0.5$, $M_{s1} = M_{s2} = 1.0$; 2.025 is found T_C/J_C. **b)** Exhibiting two successive phase transition at two different phase transition temperatures for D = −2.5 and $h = 0.5$ and the initial values of $M_{c1} = M_{c2} = M_{s1} = M_{s2} = 0.0$; 0.65 and 2.025 are found as T_t/J_C and T_C/J_C, respectively. . (For interpretation of the references to colour in this figure legend, the reader is referred to the Web version of this article.)

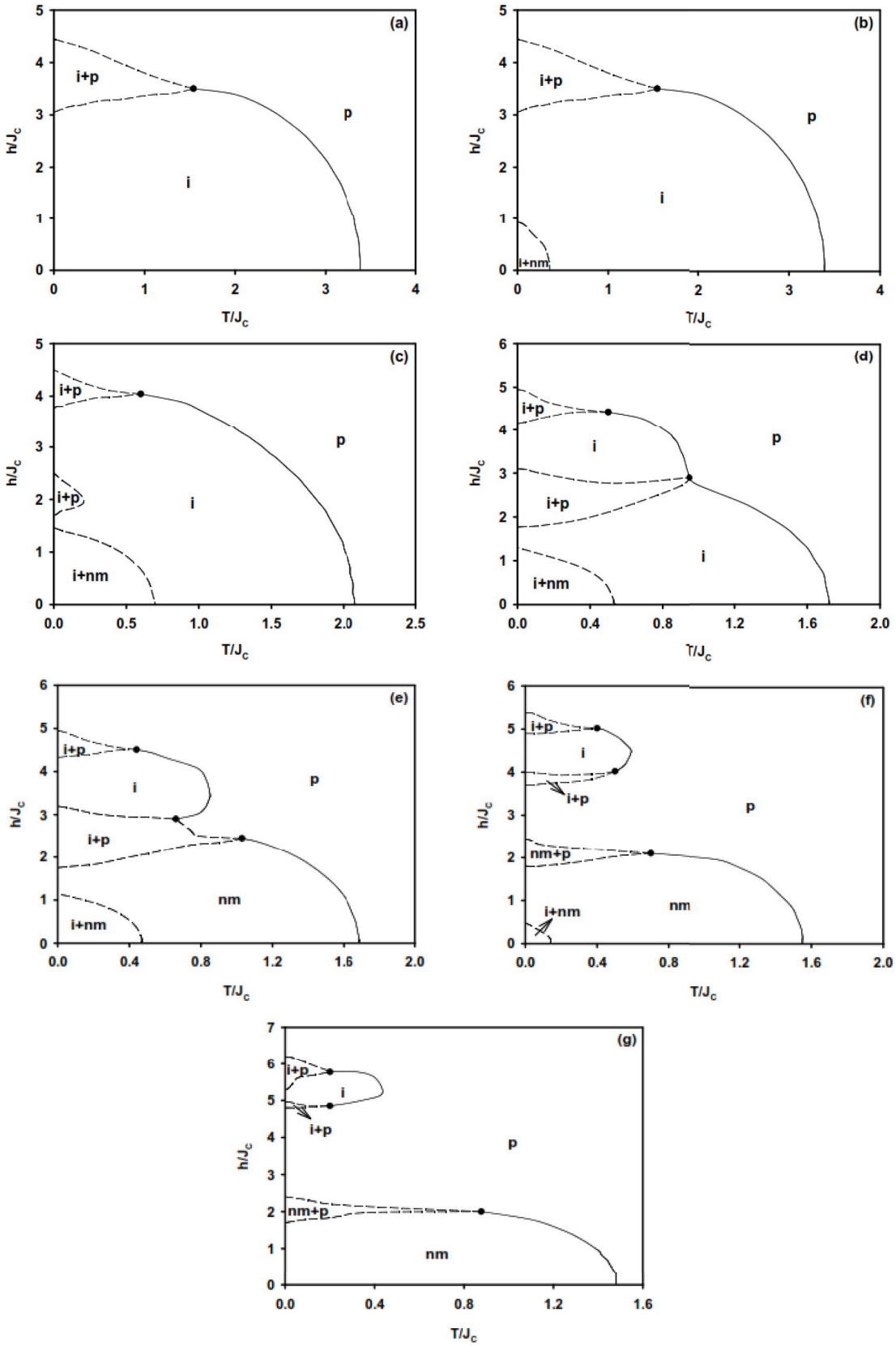

Fig. 5. The phase diagrams in the (T/J_C, h/J_C) plane for $\Delta_S = 0.0$, $r = 1.0$ and various values of the crystal field. Dashed and solid lines represent the first- and second-order phase transition temperature, respectively. The tricritical point are indicated with filled circle. **a)** $D = 1.0$, **b)** $D = -1.7$, **c)** $D = -2.5$, **d)** $D = -3.2$. **e)** $D = -3.3$, **f)** $D = -4.0$, **g)** $D = -5.0$.

solutions are paramagnetic (p); and at low values of T and h, are ferrimagnetic (i) phase. The dynamic phase boundary between these regions, i→p, is the second-order phase transition lines. At low T, there is a range of values of h in which the i and p phases or regions coexist, called the coexistence or mixed region, namely the i + p. The i + p phase is separated from the i and p phases by the first-order phase transition lines. The system also exhibits only one dynamic tricritical point where both of the first-order phase transition lines merge and signal the change from the first-to the second-order phase transition. Finally, we should also mention that the similar type of phase diagram has also obtained for $D \geq -1.115$, and is qualitatively similar to the kinetic spin-1/2 [40], spin-1 [67], spin-3/2 [43,44], mixed spin systems [42,68] and as well as different lattice models [46–49].

(ii) For $-1.115 > D \geq -1.785$ we have performed the second type of phase diagram, seen in Fig. 5(b) at $D = -1.70$. The phase diagram is similar to Fig. 5(a) but only differs from Fig. 5(a) in which low values of h and T, new mixed or coexistence region, namely i + nm, exist in the system. The phase boundary between the i and i + nm phases is the first-order line.

(iii) For $-1.785 > D \geq -3.199$ we have obtained the third type of phase diagram, seen in Fig. 5(c) at $D = -2.50$. In this case, one more mixed or coexistence region, namely i + p phase, occurs in the system at low values of T and middle values of the h.

(iv) Fig. 5(d) is illustrated for $D = -3.20$, in this case the i + p phase has grown slowly and has reached the boundary of the second-order phase transition. Moreover, the i phase has become small and the second order phase transition line has dwindled.

(v) The phase diagram is constructed for $D = -3.30$, seen in Fig. 5 (e). This phase diagram is one of the more interesting phase diagrams in which some sort of reentrant phenomenon appears at high values of h. Moreover, the phase transitions line, separated the i + p phase from the p phase, is obtained in the system. The phase diagrams present three dynamic tricritical points. The nm phase is also settled instead of the i phase at the low value of the h.

(vi) Fig. 5(f) is represented for $D = -4.0$. This phase diagram is similar to Fig. 5(e), except that the p phase has penetrated the ordered phases at the middle value of the h; hence the system exhibits three dynamic tricritical points.

(vii) For $D = -5.0$, the phase diagrams is presented in Fig. 5(g). While this phase diagram has the same pahse topology as the diagram in Fig. 5(f), it differs from Fig. 5(f) in which the i + nm phase disappears. A similar phase diagram is found to the one seen in works [43,44].

4. Summary and conclusion

In conclusion, a detailed MF investigation based on the Glauber-type stochastic dynamics has been carried out to determine the dynamical aspects (phase transitions, phase diagrams, hysteresis loop areas and correlations) of the kinetic mixed spin (1/2, 1) Ising nanowire system under a time varying (sinusoidal) magnetic field. The Glauber-type stochastic dynamics are employed to construct the set of mean field dynamic equations. The time variation of the core/shell magnetizations and the thermal behavior of the dynamic core/shell magnetizations are investigated in detail. The dynamic core/shell magnetizations, hysteresis loop areas and correlations are studied as a function of temperature in order to characterize the nature (continuous or discontinuous) of the phase transitions as well as to find the dynamic phase transition temperatures. The dynamic phase diagrams are presented in the (T/J_C, h/J_C) plane. The foremost observations reported in the present study can be briefly summarized as follows:

➢ The dynamic correlation shows shallow (negative) dip near the dynamic phase transition temparature. The dynamic phase transition temperatures have been identified as the minimum-correlation point. The hysteretic losses become maximum above the dynamic phase transition temperature. Similar magnetic behavior was obtained diverse types of magnetic systems [49,62,69,70].

➢ It was observed that the dynamic phase diagrams exhibit paramagnetic (p), ferrimagnetic (i), nonmagnetic (nm) phases, three mixed regions, (i + nm), (i + p) and (nm + p).

➢ The dynamic phase diagrams contain dynamic tricritical points and reentrant phenomena, which strongly depend on interaction parameters. In spin systems, the reentrant behavior can be identified as follows. The entropy is the crucial factor at high temperatures. The system is in the disordered phase due to the applied field. When the temperature is increased lower values, the energy and entropy are both important than entropy, and the system enters the ordered phase. As the temperature decreases lower values, the energy is important, not the entropy and the system reenter the p phase again [71]. It is also mentioning that the reentrant phenomena was observed in the dynamic substructure formation in ribonucleoprotein droplets [72], in some weakly frustrated ferromagnets, i.e. i.e. $LaSr_2Mn_2O_7$, the bulk bicrystals of the oxide superconductor $BaPb_{1-x}Bi_xO_3$ and $Eu_xSr_{1-x}S$ and amorphous-$Fe_{1-x}Mn_x$ [73–75]. The obtained results are in good agreement with some experimental and theoretical results.

As a final conclusion, much more work like this research is required to understand the experimental and theoretical findings concerning the non-equilibrium thermal and magnetic properties of the nanoparticle system in different geometries thoroughly.

Author statement

I hereby respectfully submit a revised manuscript entitled "**Nonequilibrium magnetic properties of the mixed spin (1/2, 1) Ising nanowire with core-shell structure**" with **Ref: PHYSE_2019_1363** in the light of Reviewer comments for publication in **Physica E: Low-dimensional Systems and Nanostructures**. I should also mention that the manuscript has an original and has not been previously published, is not currently submitted for review to any other journal, and will not be submitted elsewhere before one decision is made.

Declaration of competing interests

The authors declare that they have no known competing financial interests or personal relationships that could have appeared to influence the work reported in this paper.

References

[1] Y. Yüksel, Ü. Akıncı, H. Polat, Phys. A 392 (2013) 2347.
[2] A. Zaim, M. Kerouad, M. Boughrara, A. Ainane, J.J. de Miguel, J. Supercond. Nov. Magnetism 25 (2012) 2407.
[3] A. Zaim, M. Kerouad, Y. El Amraoui, D. Baldomir, J. Magn. Magn Mater. 316 (2007) e306.
[4] X.J. Chen, H.F. Xu, N.H. Xu, F.H. Zhao, W.J. Lin, G. Lin, Y.L. Fu, Z. Huang, H. Wang, M.M. Wu, Inorg. Chem. 42 (2003) 3100.
[5] A. Zaim, M. Kerouad, M. Boughrara, Solid State Commun. 158 (2013) 76.
[6] B.Z. Tian, X.L. Zheng, T.J. Kempa, Y. Fang, N.F. Yu, G.H. Yu, J.L. Huang, C. M. Lieber, Nature 449 (2007) 885.
[7] C.K. Chan, H. Peng, G. Liu, K. Mcllwrath, X.F. Zhang, R.A. Huggins, Y. Cui, Nat. Nanotechnol. 3 (2008) 31.
[8] S. Xu, Y. Qin, C. Xu, Y. Wei, R. Wang, Z.L. Wang, Nat. Nanotechnol. 5 (2010) 366.
[9] S. Nie, S.R. Emory, Science 275 (1997) 1102.
[10] A.K. Gupta, M. Gupta, Biomaterials 26 (2005) 3995.
[11] B. Gleich, J. Weizenecker, Nature 435 (2005) 1214.
[12] J. Philip, P.D. Shima, B. Raj, Appl. Phys. Lett. 92 (2006), 043108.
[13] X. Li, X. Guo, D. Wang, L. Tong, Optic Commun. 323 (2014) 119.
[14] A.E. Berkowitz, R.H. Kodama, Salah A. Makhlouf, F.T. Parker, F.E. Spada, E. J. McNiff, S. Foner, J. Magn. Magn Mater. 196 (1999) 591.
[15] X. Batlle, A. Labarta, J. Phys. D Appl. Phys. 35 (2002) R15.

[16] W.T. Coffey, D.S.F. Crothers, J.L. Dormann, Y.P. Kalmykov, E.C. Kennedey, W. Wernsdorfer, Phys. Rev. Lett. 80 (1998) 5655.
[17] S. Momose, H. Kodama, T. Uzumaki, A. Tanaka, Appl. Phys. Lett. 85 (2004) 1748.
[18] M. Vasilakaki, K.N. Trohidou, Phys. Rev. B 79 (2009) 144402.
[19] N. Nedyalkov, Y. Nakajima, M. Terakawa, Appl. Phys. Lett. 108 (2016), 043107.
[20] B.-S. Kim, S. Lee, W.-K. Kim, J.-H. Park, Y.C. Cho, J. Kim, C.R. Cho, S.-Y. Jeong, Nanoscale Research Letters 9 (2014) 22.
[21] Y. Cao, G. Wei, H. Ge, Y. Yu, Int. J. Electrochem. Sci. 9 (2014) 5272–5279.
[22] F. Tian, Z.P. Huang, L. Whitmore, Phys. Chem. Chem. Phys. 14 (2012) 8537–8541.
[23] V.S. Leite, W. Figueiredo, Physica A 350 (2005) 379.
[24] A.F. Bakuzis, P.C. Morais, J. Magn. Magn Mater. 285 (2005) 145.
[25] T. Kaneyoshi, Phys. Status Solidi B 242 (2005) 2938.
[26] T. Kaneyoshi, J. Magn. Magn Mater. 321 (2009) 3430.
[27] M. Vasilakaki, K.N. Trohidou, Phys. Rev. B 79 (2009) 144402.
[28] T. Kaneyoshi, Phys. Status Solidi B 248 (2011) 250.
[29] O. Canko, A. Erdinç, F. Taskin, A.F. Yildirim, J. Magn. Magn Mater. 324 (2012) 508.
[30] U. Akinci, J. Magn. Magn Mater. 324 (2012) 4237.
[31] V.S. Leite, B.C.S. Grandi, W. Figueiredo, Phys. Rev. B 74 (2006), 094408.
[32] T. Kaneyoshi, Phys. B 414 (2013) 72.
[33] K.R. Heim, G.G. Hembree, K.E. Schmidt, M.R. Scheinfein, Appl. Phys. Lett. 67 (1995) 2878.
[34] L.G.C. Rego, W. Figueiredo, Phys. Rev. B 64 (2001) 144424.
[35] H. Magoussi, A. Zaim, M. Kerouad, Solid State Commun. 200 (2014) 32.
[36] E. Albayrak, Phys. Lett. 380 (2016) 458.
[37] M. Boughrara, M. Kerouad, A. Zaim, J. Magn. Magn Mater. 360 (2014) 222.
[38] M. Boughrara, M. Kerouad, A. Zaim, Physica A 433 (2015) 59.
[39] E. Albayrak, J. Magn. Magn Mater. 401 (2016) 532.
[40] T. Tomé, M.J. de Oliveira, Phys. Rev. A 41 (1990) 4251.
[41] R.J. Glauber, J. Math. Phys. 4 (1963) 294.
[42] G.M. Buendía, E. Machado, Phys. Rev. E 58 (1998) 1260.
[43] M. Keskin, O. Canko, B. Deviren, Phys. Rev. E 74 (2006), 011110.
[44] B. Deviren, M. Keskin, O. Canko, Comput. Phys. Commun. 178 (2008) 420.
[45] S.A. Deviren, B. Deviren, J. Magn. Magn Mater. 402 (2016) 94.
[46] G. Korniss, P.A. Rikvold, M.A. Novotny, Phys. Rev. E 66 (2002), 056127.
[47] Y. Yüksel, E. Vatansever, H. Polat, J. Phys. Condens. Matter 24 (2012) 436004.
[48] Y. Yuksel, E. Vatansever, U. Akinci, H. Polat, Phys. Rev. E 85 (2012), 051123.
[49] M. Ertas, B. Deviren, M. Keskin, Phys. Rev. E 86 (2012), 051110.
[50] Y. Achiam, J.M. Kosterlitz, Phys. Rev. Lett. 41 (1978) 128.
[51] S.A. Deviren, E. Albayrak, Phys. Rev. E 82 (2010), 022104. S.A. Deviren, E. Albayrak, Physica A, 390 (2011) 3283.
[52] Q. Jiang, H.N. Yang, G.C. Wang, Phys. Rev. B 52 (1995) 14911.
[53] D.T. Robb, Y.H. Xu, O. Hellwig, J. McCord, A. Berger, M.A. Novotny, P.A. Rikvold, Phys. Rev. B 78 (2008) 134422.
[54] Z.A. Samoilenko, V.D. Okunev, E.I. Pushenko, V.A. Isaev, P. Gierlowski, K. Kolwas, S.J. Lewandowski, Inorg. Mater. 39 (2003) 836.
[55] K. Kanuga, M. Çakmak, Polmer 48 (2007) 7176.
[56] B. Deviren, E. Kantar, M. Keskin, J. Magn. Magn Mater. 324 (2012) 2163–2170.
[57] E. Kantar, M. Ertaş, M. Keskin, J. Magn. Magn Mater. 361 (2014) 61–67.
[58] E. Kantar, M. Ertas, Superlattice. Microst. 75 (2014) 831–842.
[59] M. Ertas, E. Kantar, Phase Transitions 88 (2015) 567–581.
[60] E. Kantar, M. Ertas, J. Supercond. Nov. Magnetism 28 (2015) 2529–2538.
[61] B. Boyarbay Kantar, M. Ertas, Phil. Mag. 98 (2018) 2734–2748.
[62] M. Acharrya, Phys. Rev. E 58 (1998) 179.
[63] A.H. Cooke, C.J. Ellis, K.A. Gehring, M.J.M. Leask, D.M. Martin, B.M. Wanklyn, M. R. Wells, R.L. White, Solid State Commun. 8 (1970) 689–692.
[64] A.H. Cooke, D.M. Martin, M.R. Wells, Solid State Commun. 9 (1971) 519–522.
[65] Z. Fisk, M.B. Maple, D.C. Johnston, L.D. Woolf, Solid State Commun. 39 (1981) 1189–1192.
[66] B. Deviren, Y. Sener, J. Magn. Magn Mater. 386 (2015) 12–19. B. Deviren, M. Keskin, Phys. Lett. A, 374 (2010) 3119-3128. B. Deviren, M. Keskin, Phys. Lett. A, 376 (2012) 1011-1019.
[67] M. Keskin, O. Canko, U. Temizer, Phys. Rev. E 72 (2005), 036125.
[68] M. Godoy, W. Figueiredo, Phys. Rev. E (2000) 61, 026111. M. Ertas, M. Keskin, B. Deviren, J. Stat. Phys., 146 (2012) 1244-1262. M. Ertas, M. Keskin, Physica A, 437 (2015) 430-436.
[69] B. Deviren, Y. Sener, M. Keskin, Physica A 392 (2013) 3969–3983.
[70] E. Vatansever, H. Polat, Phys. Lett. 379 (2015) 1568–1775.
[71] K. Hui, Phys. Rev. B 38 (1988) 802.
[72] P.R. Banerjee, A.N. Milin, M.M. Moosa, P.L. Onuchic, A.A. Deniz, Angew. Chem. Int. Ed. Engl. 56 (2017) 11354–11359.
[73] J.Q. Li, Y. Matsui, T. Kimura, Y. Tokura, Phys. Rev. B 57 (1998) R3205.
[74] T. Sata, T. Yamaguchi, K. Matsusaki, J. Membr, Science 100 (1995) 229.
[75] K. Binder, A.P. Young, Rev. Mod. Phys. 58 (1986) 801.